Journal of Materials Chemistry B

Active microfluidic reactor-assisted controlled synthesis of nanoparticles and related potential biomedical applications

Journal:	*Journal of Materials Chemistry B*
Manuscript ID	TB-REV-01-2023-000057.R1
Article Type:	Review Article
Date Submitted by the Author:	24-Apr-2023
Complete List of Authors:	Kamat, Vivek; Florida International University Dey, Preyojon; Florida International University, Mechanical and Materials Engineering Bodas, Dhananjay; Agharkar Research Institute, Nanobioscience group Kaushik, Ajeet; Florida Polytechnic University, Environmental Engineering Boymelgreen, Alicia ; Florida International University, Mechanical and Materials Engineering Bhansali, Shekhar; Florida International University,

Active microfluidic reactor-assisted controlled synthesis of nanoparticles and related potential biomedical applications

Vivek Kamat [a#*], Preyojon Dey [b#], Dhananjay Bodas [c*], Ajeet Kaushik [d, e], Alicia Boymelgreen [b], Shekhar Bhansali [a]

a. *Engineering and Computing Center, Department of Electrical engineering, Florida International University, Miami, Florida 33174, USA.*
b. Engineering and Computing Center, Department of Mechanical and Materials Engineering, Florida International University, Miami, Florida 33174, USA.
c. Nanobioscience Group, Agharkar Research Institute, G.G. Agarkar Road, Pune 411 004 India
d. School of Engineering, University of Petroleum and Energy Studies (UPES), Dehradun, Uttarakhand, India
e. NanoBioTech Laboratory, Department of Environmental Engineering, Florida Polytechnic University, Lakeland, Florida 33805, USA

E-mail: vkamat@fiu.edu; dsbodas@aripune.org
# Authors contributed equally to work.

Fabricating high-performance nanoparticles (NPs) is currently a focus of researchers due to their manipulative size-dependent unique properties needed to develop next-generation advanced systems. To harness the unique properties of NPs, maintaining identical characteristics throughout the processing and application process system is crucial to producing uniform-sized – or monodisperse NPs. In this direction, mono-dispersity can be achieved using exerting extreme control over the reaction conditions during the NP synthesis process. Microfluidic technology offers a unique approach to controlling fluid conditions at the microscale and is thus well-positioned as an alternative strategy to synthesize NPs in reactors demonstrating micrometric dimensions and advanced size-controlled nanomaterial production. These microfluidic reactors can be broadly classified as active or passive based on their dependence on external energy sources. Passive microfluidic reactors, despite their lack of reliance on external energy, are frequently constrained in terms of their mixing efficacy when compared to active systems. However, despite several fundamental and technological advantages, this area of research as well as its application to the biological sciences is not well-discussed. To fill this gap, this review for the first time discusses various strategies for synthesizing NPs using active microfluidic reactors including acoustic, pressure, temperature, and magnetic assisted microfluidic reactors. Various established ways for achieving size control on NP synthesis in microfluidic reactors represent the applicability of micro-reaction technology in developing novel nanomaterials suitable for potential biomedical application, as the focus of this review along with a comprehensive discussion about challenges and prospects.

Keywords: Microfluidics, Active microreactor, Nanoparticle synthesis, Drug delivery, External energy

1. Introduction

Nanoparticles (NPs) have attracted considerable attention in the past few decades due to their unique electrical [1], magnetic [2], mechanical [3], thermal [4], and optical [1] properties. Their small size and large surface-to-volume ratio make them valuable candidates for several applications such as drug delivery vehicles [5], electronic sensors [6], energy harvesters [7], and nanomedicine [8]. These properties of NPs are size-dependent. For example, semiconductor NPs transmit light at different wavelengths, depending on their size [9]. To ensure their consistent performance, the size of the NPs needs to be uniform or monodisperse. Monodispersity can be achieved by controlling reaction parameters such as the concentration of reagents, temperature, agitation for mixing, etc. However, traditionally most of these reactions are carried out as batch processes in large volumes which are difficult in maintaing uniform conditions throughout the process. For example, even with constant stirring, mixing by dropwise addition of one solution into another will temporarily result in the generation of gradients (concentration, temperature, pH, etc.) and non-homogeneous mixing, which then causes the resultant NPs to be polydisperse. Also, synthesis of nanoparticles is a function of reaction time, reaction kinetics and the external energy applied. Almost all the metallic nanoparticles are synthesized via reduction reactions, polymeric via ionic gelation or template assisted method and certain class of nanoparticle such as dendrimers are synthesized via controlled divergent synthesis approach. This vast diversity in reaction parameters and external factors makes monodisperse synthesis a complex process.

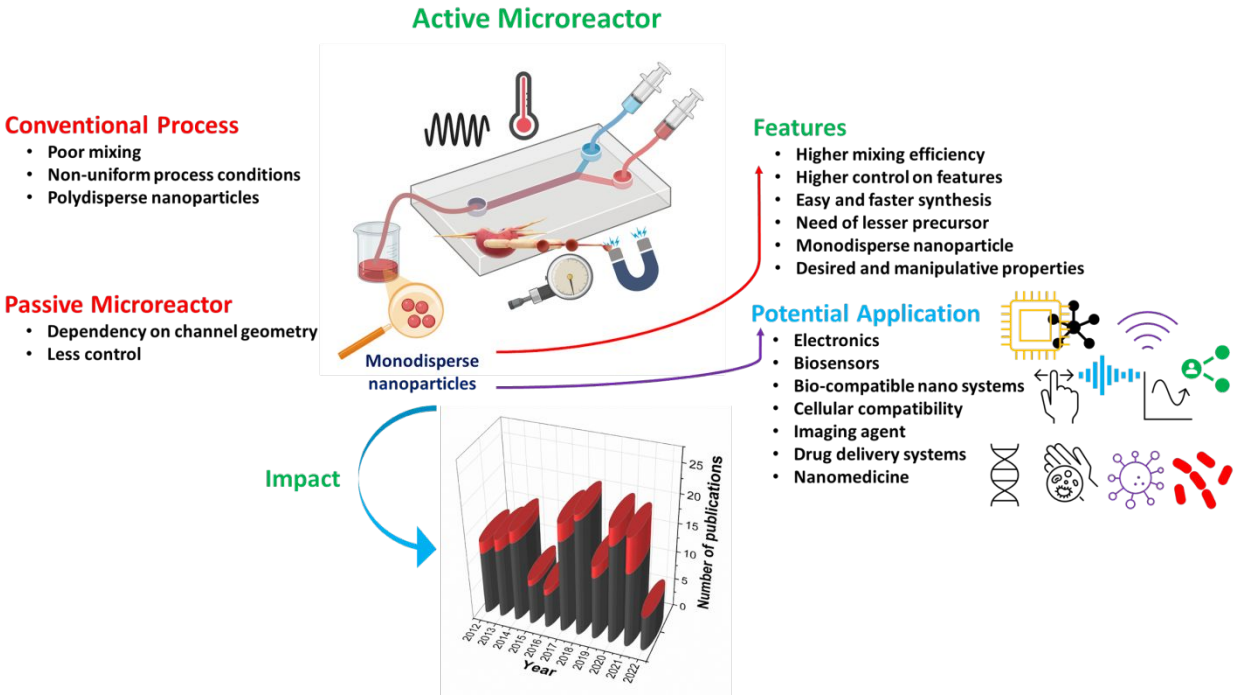

Figure 1. Overview of the use of active microfluidic reactor in the synthesis of nanoparticles for use in biomedical applications. The subset shows the trend of publications on "microfluidic reactor for nanoparticle synthesis" with varying years (the red columns show the number of publications that were based on microfluidic reactor for nanoparticle synthesis for only "biomedical applications"). The data was collected according to the keywords microreactor OR microfluidic reactor, nanoparticle synthesis, biomedical, and drug delivery from 2012-to 2022 (till 05/13/2022) (Source: Web of Science, Search Day: 05/13/2022).

In the past two decades microfluidic technology has solved much of the complexity in monodispersed synthesis via providing automation, scalability, and highly controlled microenvironments [10–20] the most important being precise control on the mixing two or more concentrations of reactants. control on reaction time (residence time) and a control on thermal gradients which form the major factors in any chemical reaction. Microfluidic reactors, defined as devices in which two or more liquids are mixed in microliter volumes exploit these properties to control reaction parameters such as temperature, intermolecular mixing, the concentration of reactants, etc. [21–26]. Many researchers have attempted to synthesize NPs using microfluidic reactors in recent years due to these virtues as is evidenced in the publishing trends over the past ten years

(2012-23) depicted in **Figure 1**. However, the synthesis of NPs by microfluidic reactors for biomedical applications is still in its infancy (Figure 1). Using microfluidic reactors to synthesize NPs for biomedical applications has promising potential in the areas of diagnostics and therapies, including cancer and infectious disease diagnosis, drug delivery, and drug discovery. Yet several key aspects such as optimum drug loading, drug nanoparticles compatibility, drug activity, shelf-life studies, biocompatibility and body clearance are yet to be fully studied, optimized and applied in real life scenario and therefore there is still much to be investigated.

As mentioned earlier flow and mixing in microfluidics systems is critical in controlling the reactions which is generally laminar, prompting the need for creative solutions to induce mixing. Microfluidic reactors for NP synthesis can be broadly divided into passive and active. Passive microfluidic reactors are primitive micromixers that mix liquids based on molecular diffusion and/or chaotic advection which is generated by the channel geometry, such as the introductions of obstacles or sharp corners [27]. Molecular diffusion can be boosted by increasing the mixing channel's length, but this result in a pressure drop in the channel [28–30]. In both cases, the mixing efficiency is still often low, challenging to regulate, and cannot be used with viscous liquids [31,32]. On the other hand, active micromixers enhance the mixing by agitating or stirring the fluid flow using externally applied energy [33,34]. Compared with passive micromixers, usually active micromixers can generate a relatively higher Reynolds number [35]. Depending on the geometry, a rise in Reynolds number leads to more intense and consequently less symmetric Dean vortices; which in turn increases the efficiency of mixing [36]. Active micromixers have also been reported to work efficiently with viscous solutions [38,39]. Therefore active micromixers are most suitable for efficient mixing (Figure 1) [32,37]. In the larger area of bio applications, active micromixers have been utilized for diagnostic applications including cancer biomarker detection [40], C-reactive protein (CRP) detection [41], sputum analysis [39], drug screening [42] and virus antibody detection [43]. However, their utilization in NP

synthesis is still in its nascent stage. Further NP-drug synthesis while maintaining monodispersity add complexity in controlling the reaction. In light of these challenges some of the research groups have attempted to synthesis NP-drug conjugate using active reactors (Table 1).

The current review centers on diverse active microfluidic reactors, their operational mechanism, and their application in the production of monodispersed NPs for biomedical applications. This review highlights requisite parameters for achieving monodisperse nanoparticles, as well as the characterization techniques employed to determine the size and shape of these NPs. The aim of this review is to provide a comprehensive understanding and generate interest towards the current techniques, technological challenges, and optimization of critical process parameters required for optimum synthesis and modification of NP for biomedical applications using active microfluidic reactors.

Table 1. Various types of microfluidic reactors, nanoparticles synthesized utilizing them, and their potential/investigated biomedical translational biomedical applications.

No.	Type of active microfluidic reactor	Type of nanoparticle (NP)	Translational application	Reference
1	Acoustic	Budesonide and DNA nanoparticles	Probable application of budesonide as asthma drug	[62]
2	Acoustic	Poly(lactide-co-glycolide)-block-poly(ethylene glycol) (PLGA-PEG), chitosan, tetrathiafulvalene (TTF)–gold (Au) hybrid, lipid/DNA complexes	Probable application of the NPs as enzyme- or drug-encapsulation	[101]
3	Acoustic	Protein nanoparticles (BCA-P114, made of bovine carbonic anhydrase (BCA) and peptide (P114))	Probable applications ranging from drug delivery and vaccines to biocatalysts and biosensors.	[102]

4	Acoustic	ZnO nanorod- Ag nanoparticles	ZnO-Ag NPs coated glass capillary used as label-free plasmonic biosensing system for detecting exosomes, DNA oligonucleotides, and E. coli bacteria	[103]
5	Acoustic	Liposome nanoshells and PLGA-PEG nanoparticles	Probable applications in controlled release systems in pharmaceutical and biomedical field	[104]
6	Pressure	Lipid nanoparticles (Gelucire 44/14)	Probable applications in cosmetic and dermatological applications due to their enhanced chemical stability, increased skin hydration effect, and prolonged release	[105]
7	Pressure	Cadmium sulfide (CdS) quantum dots	Probable applications in bioimaging in cancer therapies, diseases detection, etc. [130].	[112]
8	Pressure	Iron oxide (Fe3O4) NPs	Probable applications in bio-imaging to bio-sensing	[113]
9	Pressure	Gold NPs	Probable applications in sensing, diagnosis, biomedicine, drug delivery.	[108]
10	Thermal	Iron oxide (Fe2O3) NPs	Probable applications in drug delivery, tissue engineering, and wound healing [131].	[119]
11	Thermal	TiO2	Probable applications in nano biosensing, medical implants, drug delivery and antibacterial fields [132].	[120]
12	Thermal	UiO-66 nanoparticles [Metal-organic frameworks (MOFs)]	drug delivery behavior for 5-fluorouracil (5-Fu) with UiO-66 NPs was investigated	[117]
13	Thermal	Au–Ag alloy nanoparticles	Probable applications in biosensing, and drug delivery [133].	[118]

14	Thermal	SnO2 nanoparticles	Probable applications in respiratory and cancer diseases for gas detection [134].	[122]
15	Magnetic	chitosan nanoparticles	Drug (amphotericin B) loading, release, and testing on MCF-7 cells (In-vitro)	[54]
17	Magnetic	Benzathine Penicillin G tetrahydrate (BPG)-TiO2 NPs	Antibacterial activity measured on S. aureus, a Gram-positive bacterium (in-vivo)	[129]

2. Mechanism of synthesis of nanoparticles and influence of confined volumes

To comprehend the nanoparticle synthesis process, LaMer and Dinegar developed the LaMer plot (Figure 2), which describes the events occurring during synthesis [44]. According to LaMer et al., monomer precursors are formed in stage I. When the concentration of the monomer precursor reaches the nucleation threshold (or critical concentration for nucleation), self-nucleation starts to occur (stage II). As the reaction proceeds, the monomer precursor concentration drops below the threshold. Finally, the growth of the nuclei (stage III) is initiated by the total consumption of the monomer precursors in the solution. In other words, the first nuclei are formed when the monomer precursor concentration of the reaction reaches a critical concentration for nucleation. This process is followed by the growth of the core above the solubility limit. Ultimately the concentration becomes close to saturation, and growth ends. The separation of nucleation and growth events is imperative to obtain monodispersity (Figure 2). Otherwise, particles nucleated at an earlier stage will grow larger than those nucleated later. The nucleation and growth events can be separated by controlling the concentration of monomer precursors such that they are above the solubility limit but below the critical concentration for nucleation. Specifically, the concentration should not reach the nucleation threshold during the growth stage to avoid temporal differentiation of nuclei

generation. The monomer precursor formation can be controlled by monitoring the reaction conditions such as pH, temperature, or supply of reactants [45]. For example, where the reaction requires heat, as in the case of thermal decomposition reactions, rapid changes in the temperature can be used to control the rate of monomer precursor formation [46]. When the system's pH is reduced rapidly, the reaction will be quenched, which can be used to control the time of the nucleation stage [47]. In all the methods where reactions require rapid pH change and high temperature of mixing of reagents, it is essential to control the reaction conditions uniformly throughout the system such that monodisperse nanoparticles can be achieved.

In a conventional batch reaction, maintaining this level of control can be arduous. On the other hand, micromixers deal with small volumes offering the possibility of precise control of the reaction parameters. Due to homogeneous mixing in microfluidic reactors, the mixing is faster [48]. Therefore, microfluidic reactors are very appealing, especially for reactions with high-speed

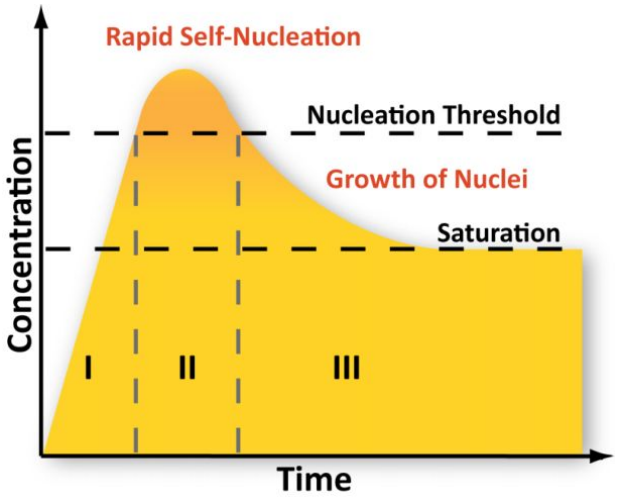

Figure 2. La-Mer's plot represents the concentration profile required for the monodisperse synthesis of nanoparticles.

kinetics or for dealing with unstable intermediate substances. Moreover, spatial and temporal monitoring and controlling of reactions can be attained by adding reagents at precise time intervals

during the reaction progress. The fast-mixing process has a valuable advantage in precipitation/crystallization processes such as the production of colloidal systems or nanoparticles. Researchers have demonstrated the synthesis of metallic [25,49–51], polymeric [52–56], and semiconductor [57,58] nanoparticles using micromixers .

3. Principles of mixing using microfluidics and active mixing

Active mixing is governed by the fluid momentum and mass transport equations. The Navier-Stokes equation expresses the conservation of momentum for incompressible fluid flow, and is expressed by the equation-

$$\rho\frac{\partial\vec{u}}{\partial t} + \rho\vec{u}.\nabla\vec{u} = -\nabla p + \eta\nabla^2\vec{u} \quad (1)$$

where t is time[sec], ρ is fluid density [kg/m^3], $\vec{u}$ is velocity vector [m/sec], and p is pressure [Pa] [59].

Which can be rewritten in nondimensional form-

$$Re\frac{\partial\vec{u}^*}{\partial t^*} + Re\,\vec{u}^*.\nabla^*\vec{u}^* = -\nabla^* p^* + \nabla^{*2}\vec{u}^* \quad (2)$$

where, $\nabla^* = \frac{\nabla}{1/l}$, $\vec{u}^* = \frac{\vec{u}}{U}$, $t^* = \frac{tU}{l}$, U is characteristic velocity, and Re is Reynolds number that determines the type of fluid flow. Physically, the Reynolds number represents the ratio of inertial force to viscous force within a fluid and is expressed by-

$$Re = \frac{U\,l}{\nu} \quad (3)$$

where l, and ν are characteristic length [m], and kinematic viscosity [m^2/sec], respectively [59]. The convection-diffusion transport equation governs molecular advection-

$$\frac{\partial c}{\partial t} + \vec{u}.\, c^{*}\ \nabla c = D\nabla^2 c \quad (4)$$

where c, $\vec{u}$, and D, are the species concentration, velocity vector, and diffusion coefficient, respectively.[65]

It can be also expressed in nondimensional form-

$$\frac{\partial c^{*}}{\partial t^{*}} + \overrightarrow{u^{*}}.\nabla^{*} c^{*} = \frac{1}{Pe} D\nabla^{*2} \quad (5)$$

where $c^{*} = c/C$ (C= characteristic concentration) and Pe is Peclet number, which is the product of Reynolds number and Schmidt number (ratio of the kinematic viscosity to the molecular diffusion coefficient) and physically represents the ratio of mass transport due to convection to that of diffusion. It is expressed by the equation-

$$Pe = \frac{Ul}{D} \quad (6)$$

The diffusion coefficient, D, can be calculated from the Stokes-Einstein equation-

$$D = \frac{RT}{N} \cdot \frac{1}{6\pi Z r} \quad (7)$$

where R, T, N, Z, and r are the gas constant [8.3145 J/mol.K], absolute temperature [K], Avogadro's number [6.023×10^{23} mol^{-1}], viscosity of the medium [Poiseuille, or, kg/m.sec], and the radius of a diffusing particle [m] [60].

Reynolds number determines the type of fluid flow. In a microfluidic channel, the Reynolds number is very low due to the smaller channel size; thus, the flow is laminar, and there is no turbulence to induce mixing. On the other hand, at the microlevel, the Peclet number is very high, which means minimal diffusion. These conditions make it very challenging for mixing in micro dimensions. The mixing quality of a micromixer can be improved by increasing the fluid's diffusion coefficient, which can be accomplished by employing a higher temperature and/or smaller diffusing particles. Increasing the concentration difference between the mixing fluids and surface area can also promote diffusion. However, these approaches are often still not sufficient to obtain complete

homogenization. Shortening diffusion length can maximize the mixing. In microfluidic devices, this is usually obtained by using chaotic mixing which reduces the characteristic length exponentially. The fluids are forced to flow randomly through chaotic advection (using external energy in active micromixer and channel design in passive micromixer), generating random pressure and velocity variations within the fluid concerning space and time. As a result, the interfacial area between the species increases, and the species mix more efficiently [61,62]. Overall, active mixing utilizes external energy to induce chaotic advection, generate disruption, shorten diffusion length, increase the contact area between species, and strengthen the mixing effect. Consequently, an active mixer provides superior mixing in a compact space throughout a broad range of Reynold numbers. With the smaller volume, microfluidic reactors will require fewer reactants and be more cost- and time-effective.

4. Synthesis of nanoparticles using active micromixers for biomedical applications

Conventional drug delivery systems cannot yield the optimal therapeutic impact mainly due to the rapid metabolism, poor absorption, poor bioavailability, and early excretion from the bod [63,64]. A single dosage cannot maintain a consistent medication level, necessitating administering several doses at regular intervals. The dosing regimen raises the likelihood of variable doses (low or high), resulting in toxicity and inefficacy. Consequently, innovative approaches for the regulated release of pharmaceuticals are being developed. Due to their adaptable physiochemical characteristics, nanoparticles are used widely for biomedical applications, particularly drug delivery [65,66], magnetic hyperthermia [67,68], diagnostics [69], imaging [70], etc. Using nanoparticles to carry drugs to hard-to-reach areas and release them in a regulated way allows for better drug distribution and dose for a higher therapeutic impact [71–73]. They can be effectively adsorbed on the cell membrane with the

help of surface ligands and thus can avoid early excretion [74]. They can also be used for magnetic hyperthermia, where electromagnetic energy is used to heat targeted cancer cells [75,76]. Nanoparticles are also used with contrast agents for bioimaging [61,70,77]. Nanoparticles also find wide application in biosensors when coated with bio responsive elements such as enzymes, nucleic acids, antibodies, etc. [78–80]. Due to their unique properties, such as chemical inertness, biocompatibility, high magnetic susceptibility, high saturation magnetization, and the ability for surface functionalization, magnetic nanoparticles, such as Fe_3O_4 [81–84], Au [85–88], Ag [89–91], Fe-Co [92–94], etc., are the most widely utilized in biomedical applications. However, these ultrasensitive biomedical applications need highly monodisperse nanoparticles to guarantee uniform biodistribution, and homogeneous surface functional groups [74]. Active mixing gives excellent control, a faster rate, and greater efficiency, but it is not often employed in microfluidic reactors for nanoparticle synthesis, owing to the complex fabrication process. However, active microfluidic reactors promise the synthesis of highly monodisperse nanoparticles with novel features [95,96]. Consequently, it is crucial to explore different types of active microfluidic reactors reported in scientific literature for producing nanoparticles for biomedical applications. Active microfluidic reactors can be classified as acoustic, pressure, temperature, or magnetic, based on the external energy employed.

4.1. Acoustic-assisted microfluidic reactor approach to develop nanoparticles

In this type of active mixer, mixing is achieved by imparting acoustic energy to the channels, which create turbulence in the liquid. Acoustic waves are transmitted via piezoelectric devices, which generate acoustic waves when an electrical voltage is applied. The advantages of acoustic microfluidic reactors include rapid mixing, fine-tuned control over the mixing process, and the capacity to handle sensitive biological materials [97–99]. A few studies reported that active

microfluidic reactors assisted by acoustic energy were used to synthesize nanoparticles for biomedical applications [62,100–105].

Le et al. developed an acoustically actuated microfluidic reactor, providing high mixing efficiency and a high flow rate [62]. The device consists of an oscillator plate that can be actuated using a piezoelectric transducer (Figure 3A). This plate is sandwiched between two PDMS channel layers where two liquids are perfused in the bottom layer, and the mixed solution is passed through the top layer to the outlet. The device has a mixing efficiency of 91%, and the flow rate can reach even up to 10 mL/min. Using this device, two different types of nanoparticles were synthesized (Budesonide and DNA nanoparticles). Budesonide is an asthma drug, and with this platform, its nanoparticles were synthesized with a small size distribution (80.53-97.03 nm) with concentrations as high as 4 mg/mL. Also, DNA nanoparticles of average sizes ranging from 60-200 nm could be synthesized using this platform by varying the flow rate (Figure 4A-a). Although the mixing index reduced at a higher flow rate, the smaller size of the particles was achieved. The particle size was

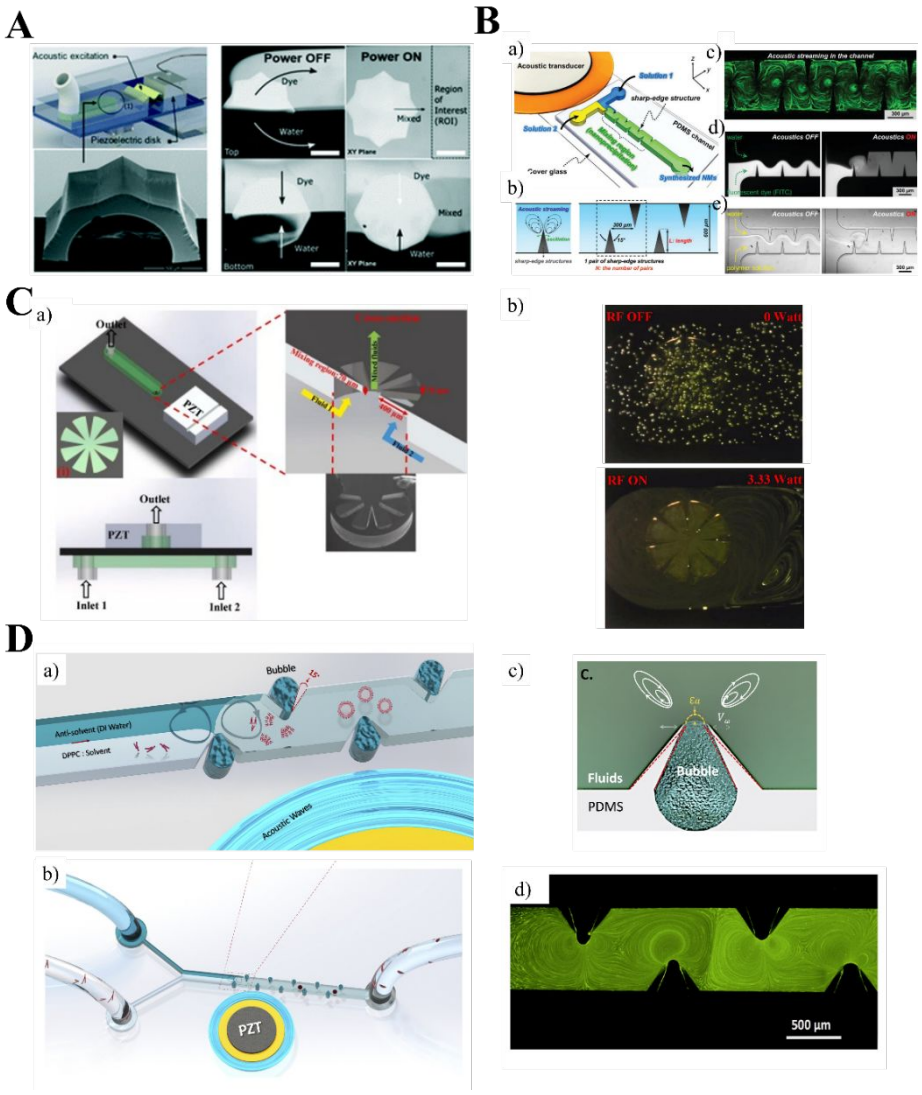

Figure 3. Acoustic-assisted assisted microfluidic reactor for nanoparticle synthesis. (A) Acoustic microfluidic reactor with star-shaped piezoelectric actuator applied to synthesize Budesonide and DNA nanoparticles [62]. (Reproduced from Ref. [62] with permission from the Royal Society of Chemistry.) (B) Schematic diagram of- (a) acoustofluidic microfluidic reactor with sharp-edge structures for nanoparticle synthesis, (b) acoustic streaming due to sharp-edge, (c) acoustic streaming induced in the fluorescent dye, and (d,e) Flow field of the species before and after the application of acoustic energy [101]. (Reproduced from Ref. [101] with permission from the Wiley.) (C) Schematic diagram of (a) Acoustic microfluidic reactor with lotus-shaped actuator for Poly lactide-co-glycolic acid (PLGA) nanoparticle synthesis, (b) Acoustic streaming with and without acoustic field [106]. (Reproduced from Ref. [106] with permission from the Elsevier.) (D) Schematic of (a) Acoustic field and bubble-assisted microfluidic reactor for nanoparticle synthesis, (b) Acoustofluidic microfluidic platform, (c) Combined unit of acoustic field and entrapped bubble due to sharp-edge, (d) Fluid flow pattern because of the combined effect of acoustic field and bubble [104]. (Reproduced from Ref. [104] with permission from the Royal Society of Chemistry.)

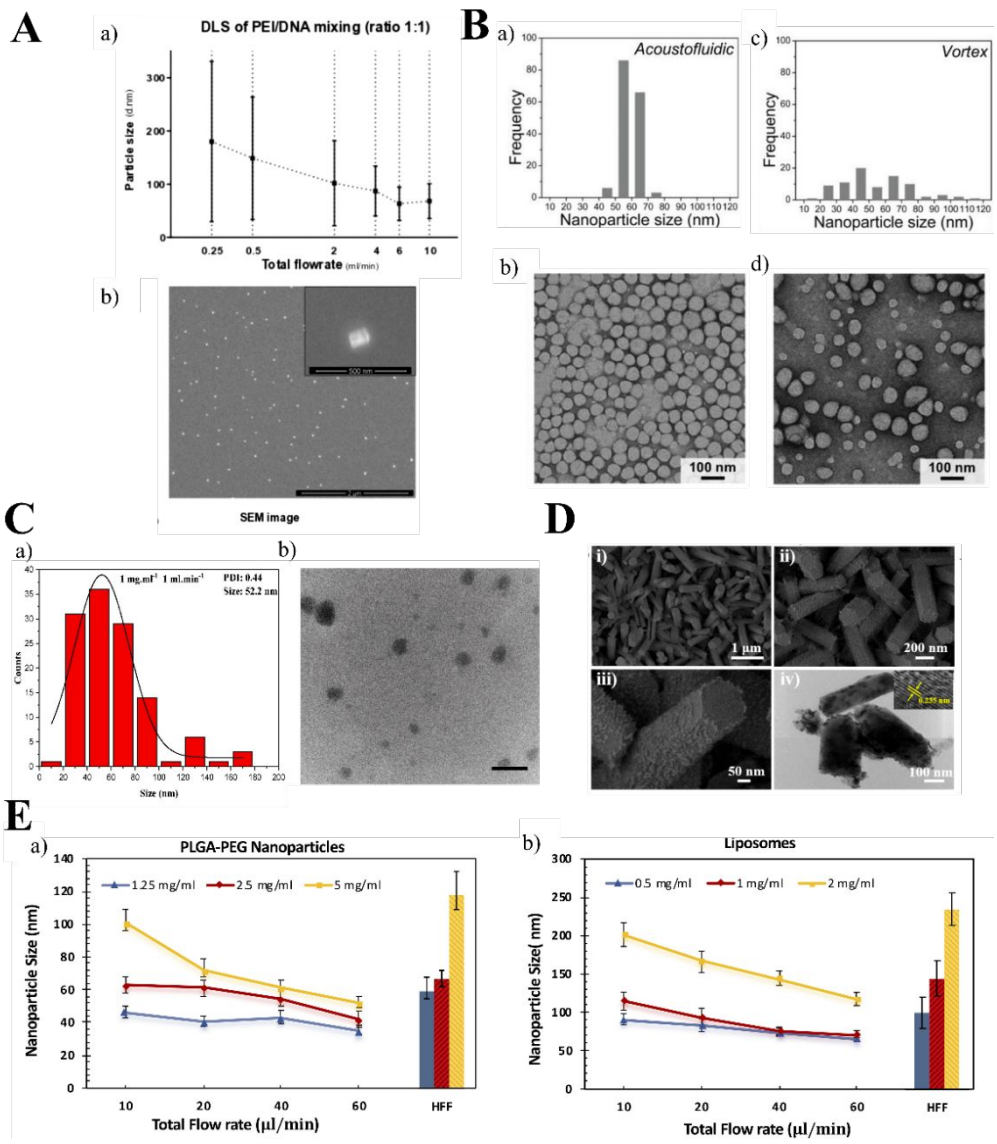

Figure 4. Characterization of nanoparticle size synthesized using acoustic field-assisted microfluidic reactor. (A) Synthesis of different sizes of nanoparticles with different flow rates (a), SEM images of nanoparticles synthesized using flow rate 6 mL/min (b) [62]. (Reproduced from Ref. [62] with permission from the Royal Society of Chemistry.) (B) Size distribution and TEM images of PLGA-PEG nanoparticles synthesized using (a, b) acoustofluidic microfluidic reactor and (c,d) vortex mixer [101]. (Reproduced from Ref. [101] with permission from Wiley.) (C) Size distribution (a), and TEM image (b) of synthesized PLGA nanoparticles [106]. (Reproduced from Ref. [106] with permission from the Elsevier.) (D) SEM (i, iii) and TEM (ii, iv) images of the synthesized ZnO-Ag nanoparticles [103]. (Reproduced from Ref. [103] with permission from the American Chemical Society.) (E) Synthesis of different sizes of (a) PLGA-PEG nanoparticle, (b) Liposome nanoparticles in acoustic assisted microfluidic reactor by changing flow rate (consequently mixing time) and comparison with the size of the nanoparticles synthesized using hydrodynamic flow focusing (HFF) [104]. (Reproduced from Ref. [104] with permission from the Royal Society of Chemistry.)

determined by using a dynamic light scattering system (DLS). Their morphology was observed under a scanning electron microscope (SEM) (Figure 4A-b), and their size distribution was also calculated by the ImageJ program using SEM images.

In another study, Huang et al. constructed a microfluidic reactor made of single-layer polydimethylsiloxane (PDMS) with a channel containing sharp-edge protruding features (Figure 3B) on the sidewalls [101]. Additionally, the device includes a cover glass and an acoustic transducer. When electrical energy is applied to the transducer, the sharp-edge features oscillate, and the species mix due to the counter-rotating vortices generated. With this device, a quick homogenization of fluorescent dye and deionized water (DIW) was achieved within ~80 ms. With this device, several types of nanoparticles were synthesized: poly(lactide-*co*-glycolide)-block-poly (ethylene glycol) (PLGA-PEG), chitosan, tetrathiafulvalene (TTF)–gold (Au) hybrid. Also, the synthesis of lipid/DNA complexes was performed. The mixing efficiency is directly related to the acoustic field and the length of sharp-edge structures in the channel. A driving voltage of 20 Vpp, a frequency of 4 kHz, and sharp-edge structures of 300 μm in length resulted in the miniature and uniform nanoparticles. Also, the number of sharp-edge structures affects the nanoparticle size. When the number varied from 2 to 13 pairs, the NP size also ranged from 102.8 ± 1.2 to 88.61 ± 0.6 nm, improving almost 40% in polydispersity index (PDI). Moreover, this study showed that non-spherical nanoparticles could also be synthesized with this device. TTF-Au hybrid nanoparticles of different shapes (square/rectangular, crosses with dendrite, and wire-like) by changing the flow rate ratio of TTF and $HAuCl_4$. The size distribution of the nanoparticles was measured by using DLS at room temperature and morphology was examined by SEM and transmission electron microscopy (TEM) [Figure 4(B)].

Pourabed et al. used a star-shaped acoustic microfluidic reactor [Figure 3(C)] with a variable thickness silicon resonator to synthesize protein nanoparticles (BCA-P_{11}4, made of bovine carbonic anhydrase (BCA) and peptide (P_{11}4)) [102]. It was reported that after utilizing the acoustic actuation, the synthesized nanoparticles became more monodisperse (PDI: 1 to 0.38), and DLS results showed that their size reduced from 207.2 ± 207.5 nm to 149.6 ± 56.5 nm [Figure 4(C-a)]. The mixing index was reported to be as high as approximately 85%. In another study by the same author, acoustically driven and hydrodynamically coupled cantilevers were used as resonators for mixing fluids [106]. The device could mix fluids efficiently (90%) with a very high flow rate (1400 μL/min) within 2 ms. TEM was utilized to examine the morphology and size distribution of the nanoparticles [Figure 4 (C-b)]. Small (52 nm) and monodisperse (PDI: 0.44) Poly (lactide-co-glycolic acid) (PLGA) nanoparticles were synthesized using this platform, which is usually used for drug delivery applications.

In another study by Hao et al., an acoustofluidic platform was developed, consisting of an acoustic transducer, and a microfluidic channel with sharp-edge structures [103]. This platform was utilized to synthesize ZnO nanorods and pattern them on the inner wall of a glass capillary. SEM and TEM were utilized to investigate the morphology of the synthesized particles [Figure 4(D)]. When silver (Ag) nanoparticles were deposited onto the ZnO nanorods, it acted as a biosensor to detect exosomes, DNA oligonucleotides, and E. coli bacteria.

Rasouli et al. incorporated oscillating bubbles into the sharp-edge structures of a microfluidic channel embedded with a piezoelectric transducer [Figure 3(D)] [104]. The volume of the gas entrapped in the bubble can be pulsated; thus, it acts as a secondary acoustic transmitter. Also, the

combination of bubble and sharp edges functions as oscillating boundaries together in the presence of an acoustic field and is thus found to strengthen acoustic streaming. With this device, almost 90% mixing index was achieved with a flow rate of 116 μL/min within 0.8 ms. Monodisperse liposome nanoshells and PLGA-PEG nanoparticles could be synthesized with this platform. Their size was measured by using DLS [Figure 4(E)] and their monodispersity was confirmed by TEM.

4.2. Pressure-assisted microfluidic reactor Approach to Develop Nanoparticles

In this type of microfluidic reactor, external pressure sources are applied to induce positive or negative pressure to create a disturbance within the fluids and thus cause mixing. This type of oscillator usually uses pulsatile forces for mixing the species involved. Only a very few studies have used this type of microfluidic reactor to synthesize nanoparticles, let alone for biomedical applications [107–111].

Xia et al. developed a microfluidic oscillator using an elastic diaphragm that deflects downward due to pressure created by a pressure pump and upward by its elastic force and hydrodynamic lift force [Figure 5(A)] [105]. The up and down motion of the diaphragm induces disturbance in the fluid and causes mixing. High drug loading and stability, precise release control, and minimal toxicity make lipid nanoparticles appealing for drug delivery. This microfluidic reactor synthesized monodisperse (PDI: 0.16-0.26) solid lipid nanoparticles (SLN). The size distribution of the nanoparticles was measured by using DLS method [Figure 6(A)]. The size of SLN was dependent on microfluidic reactor chamber depth, pumping pressure, etc.

In the study by Wang et al., the synthesis of quantum dots was demonstrated using a pneumatic micromixer [Figure 5(B)] [112]. Quantum dots are regarded as outstanding probes for bioimaging

applications. The synthesis process involved imparting a gas pressure of 0.26 MPa on a 100 μm-thick polydimethylsiloxane (PDMS) pneumatic diaphragm, which caused mixing. The mixing of fluids with flow rates ranging from 1 to 650 μL/min was achieved at a pumping frequency of 50 Hz. UV-vis results show that, monodisperse Cadmium sulfide (CdS) quantum dots were synthesized using these optimized parameters with controlled size and distribution [Figure 6(B)].

Lee et al. developed a pneumatically actuated microfluidic reactor consisting of a double-loop rotary micromixer, two micropumps, and one microvalve [Figure 5(C)] [113]. The device is made of 2 layers of PDMS and a glass substrate for sealing purposes. The top layer has air chambers and is connected to an external air pressure source, and the bottom layer acts as a pump by deflecting downwards sequentially due to air pressure. This microfluidic reactor showed 98% mixing efficiency within 2 sec with 15 psi applied pressure, driving frequency of 7.67 Hz, and pumping rate of 300 μL/min. Because of its excellent chemical resilience, cytocompatibility, non-toxicity, and high magnetic susceptibility, iron oxide has been extensively employed for drug delivery, bioimaging, and cell labeling. With this microfluidic reactor monodisperse iron oxide nanoparticles could be synthesized. The size distribution of the synthesized nanoparticles was measured using TEM and software (SigmaScan, Systat Software, USA) [Figure 6(C)].

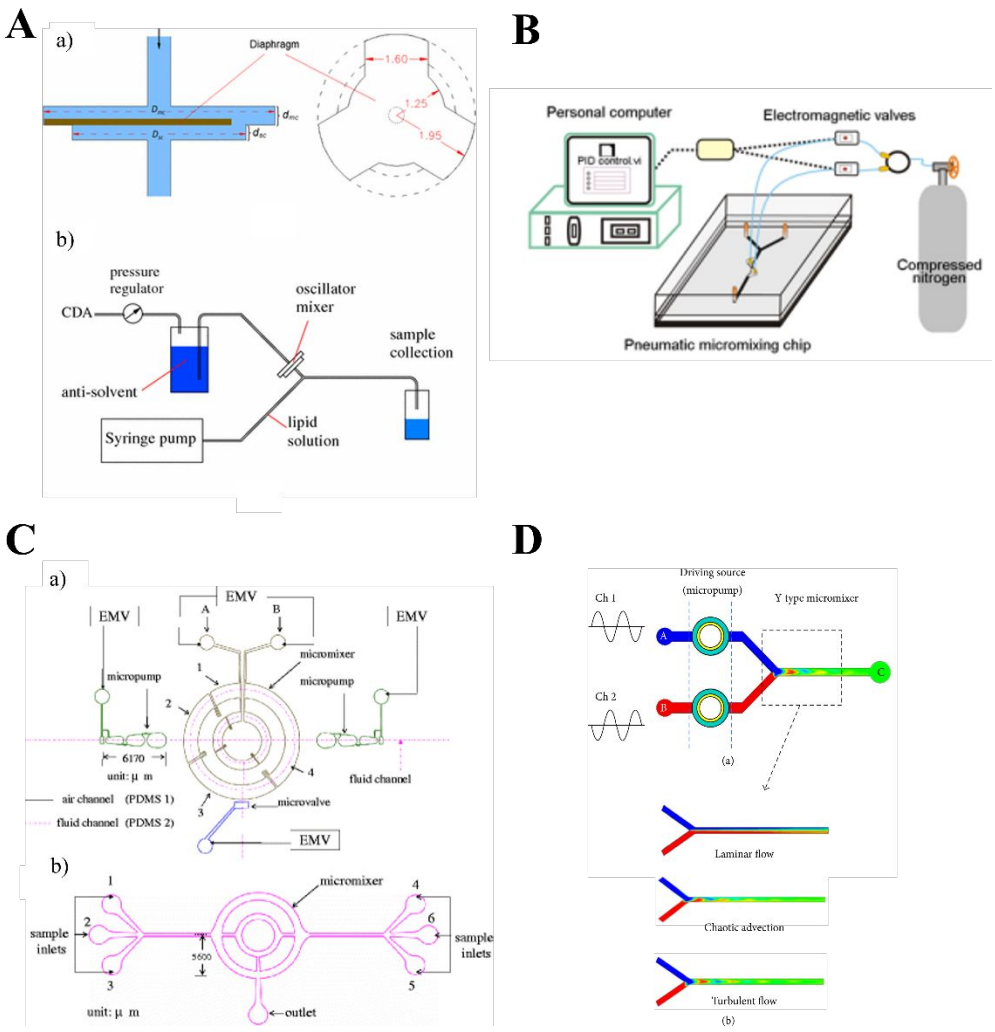

Figure 5. Pressure-assisted active microfluidic reactor for nanoparticle synthesis. (A) Schematic of (a) pressure-assisted microfluidic reactor made of a diaphragm, b) schematic of the synthesis of nanoparticles using this microfluidic reactor [105]. (Reproduced from Ref. [105] with permission from the Springer Nature.) (B) Schematic diagram of a pneumatic pressure-assisted microfluidic reactor [112]. (Reproduced from Ref. [112] with permission from the Springer Nature.) (C) Schematic diagram of microfluidic reactor (a) The first layer contains micropumps, a microvalve, and a micromixer; (b) The second layer has fluid channels for sample input [113]. (Reproduced from Ref. [113] with permission from the Springer Nature.) (D) Diagram of (a) Pulsed micromixing; b) Types of mixing modes resulting from pulse mixing [108]. (Reproduced from Ref. [108] with permission from the Hindawi.)

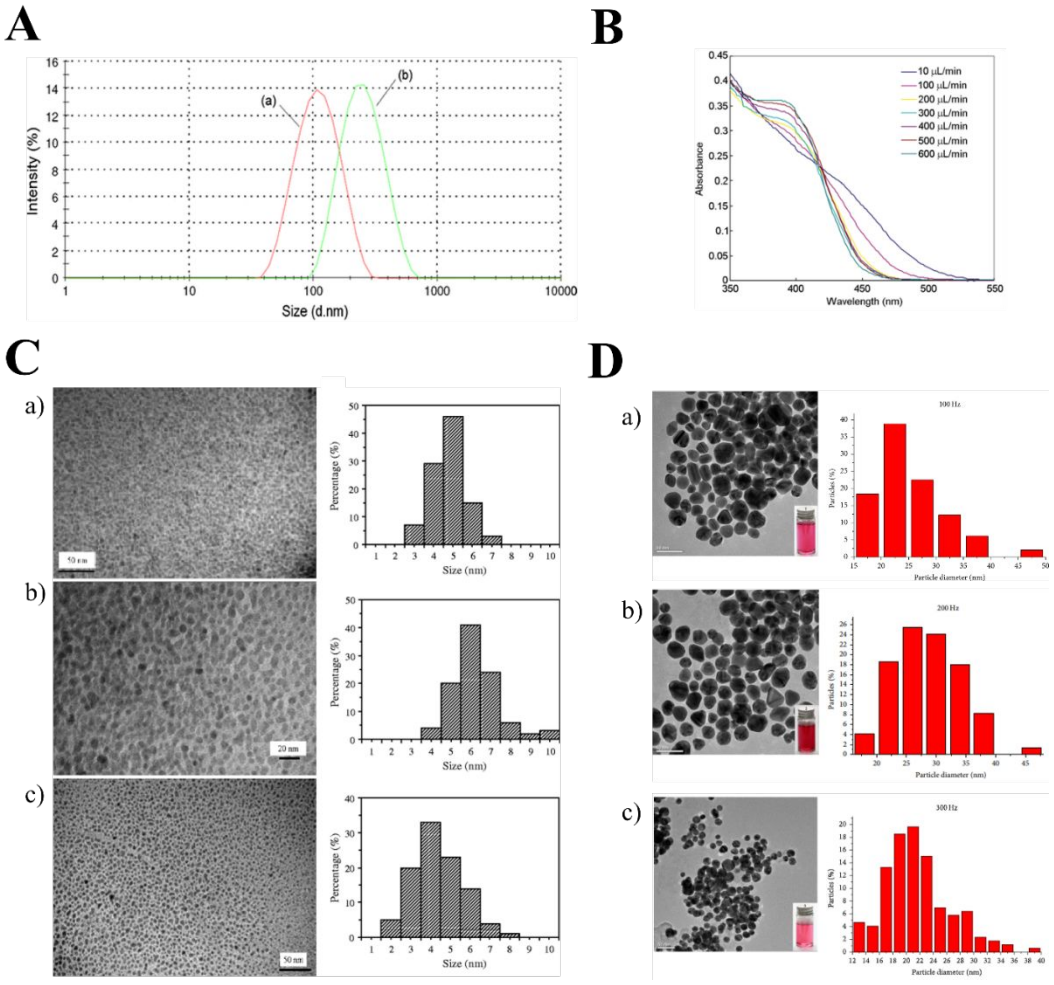

Figure 6. Characterization of nanoparticle size synthesized by utilizing pressure-assisted microfluidic reactor. (A) Size distribution of SLN nanoparticle measured by DLS method, synthesized at different pressures (a) 4.5 bar, and (b) 6 bar [105]. (Reproduced from Ref. [105] with permission from the Springer Nature.) (B) As UV-vis curve become steep, the CdS quantum dot nanoparticles become more monodisperse [112]. (Reproduced from Ref. [112] with permission from the Springer Nature.) (C) TEM images and size distribution of the synthesized iron oxide nanoparticles at three different precursor combinations [113]. (Reproduced from Ref. [113] with permission from the Springer Nature.) (D) TEM and size distribution of the nanoparticles synthesized at different pulsing frequencies [108]. (Reproduced from Ref. [108] with permission from the Hindawi.)

A pulsed micromixing (Liu et al.) method was shown in which a PZT micropump is used to provide mixing power for a Y-type micromixer [Figure 5(D)] [108]. The pulsing fluid fields cause rapid stretching and folding of the fluid interfaces, which causes the different modes of mixing laminar,

chaotic, and turbulent flow. Synthesis of gold nanoparticles was demonstrated using this micromixer. Solution A containing chloroauric acid and solution B containing sodium citrate were passed through channels one and two. The reaction led to the formation of gold nanoparticles in the micromixer with an average size of 25 nm. The pulse frequency modulates the nanoparticles' size. The morphology of the nanoparticles was characterized by TEM, and from the TEM images their size distribution was calculated using ImageJ program [Figure 6(D)].

4.3. Thermal-assisted microfluidic reactor Approach to Develop Nanoparticles

Mixing achieved using thermal energy is categorized under thermal micromixers [109,110]. Nanoparticles that require heat during synthesis can be produced using such kinds of micromixers [111]. Also, joule heating can induce temperature difference within the fluid resulting in permittivity and conductivity gradient, which causes disturbance in fluid and thus mixing [Figure 7(A)] [114]. Electrothermal forces were also applied to generate mixing; as reported by Huang et al., a non-uniform A.C. electric field was applied across the microchannel, which caused an electrothermal force on the fluid flow, leading to generating of vortex enhancing mixing [115].

In another report, the mixing of biochemical reactions was performed by conventional currents created due to an externally applied temperature in a microfluidic chamber [116]. The work highlights micromixing and subsequent polymerase chain reaction (PCR) for an influenza viral DNA fragment. However, several publications on thermally assisted micromixing have been relatively few reports on its usage for manufacturing nanoparticles and even fewer for biomedical applications.

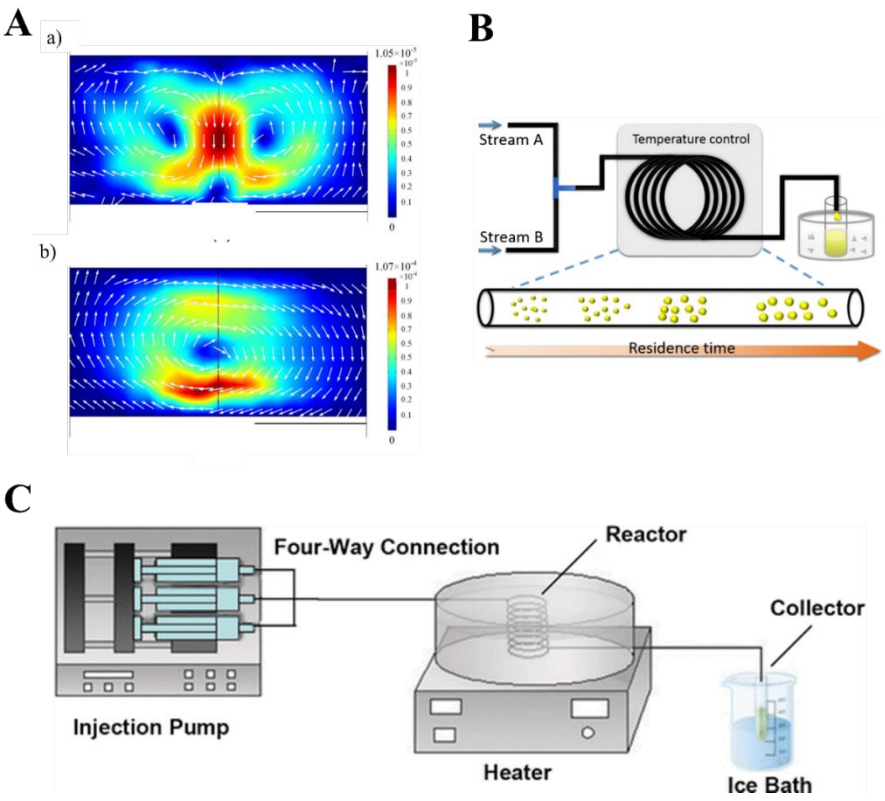

Figure 7. Temperature-assisted active microfluidic reactor for nanoparticle synthesis. (A) Velocity distribution on the cross-section of a microchannel (a) without electrode heater and (b) with the heater [114]. (Reproduced from Ref. [114] with permission from the SAGE Publications.) (B) Schematic view of the continuous flow microfluidic reactor for nano- UiO-66 [117]. (Reproduced from Ref. [117] with permission from the Elsevier.) (C) Schematic of Au-Ag nanoparticle synthesis by using a thermal assisted microfluidic reactor [118]. (Reproduced from Ref. [118] with permission from the Springer Nature.)

There have been reports on synthesizing nanoparticles using such reactors, some of which involve the continuous hydrothermal synthesis of Fe_2O_3 nanoparticles [119]. The synthesis was carried out at 673 K and 30 MPa using a T-type micromixer and a central collision-type micromixer (CCM). The CCM kind of micromixer avoids heterogeneous nucleation, which occurs on the inner wall of the mixer. The CCM micromixer effectively worked to produce smaller and monodisperse Fe_2O_3 nanoparticles, supported by their TEM images.

Park et al. reported the synthesis of TiO_2 particles by thermal decomposition of titanium tetra-isopropoxide (TTIP) in a nitrogen carrier gas with decomposition temperatures from 300°C to 1000°C [120]. The micromixer converts an aerosol precursor to solid particles by evaporating TTIP. The nanoparticle aggregates produced in the reactor are sampled by deposition on an electron micrograph grid at the reactor exit, the size of which was in the range of 200 to 400 nm.

A glass micromixer has also been fabricated for high-temperature reactions required to synthesize high-quality quantum dots, exhibiting excellent chemical and thermal durability. Heating is achieved by placing the chip on a hot plate, facilitating quantum dots synthesis [121]. The TEM and absorption-emission spectra of the synthesized quantum dots revealed high monodispersity [Figure 8(A)]. Tai et al. have synthesized a metal-organic framework (MOF) nanoparticle: UiO-66, using a microfluidic reactor [Figure 7(B)] [117]. UiO-66 is prepared by batch production conventionally but cannot produce particles on nanoscale due to a lack of control of the synthesis process [Figure 8(B)]. They have utilized a continuous flow microfluidic reactor in this study, providing superior control of mass feeding, reaction temperature, and time. The microfluidic reactor consisted of a T-mixer where two different streams of solution collide and flow through a coil of channels where the temperature was at 120ºC. The output was precipitated at the outlet. NH_2 functionalized UiO-66 nanoparticles were synthesized by this microfluidic reactor to test drug delivery of 5-fluorouracil (5-Fu) in PBS solution. It was reported that the nanoparticles could release up to 75.06% 5-Fu within 24 hours.

Au, Ag nanoparticles have wide applications in biomedicine. Liu et al. synthesized Au-Ag alloy nanoparticles using a tubular microfluidic reactor by reduction reaction of $HAuCl_4$ and $AgNO_3$ in the presence of Cacumen Platycladi (C. Platycladi) [Figure 7(C)] [118]. $HAuCl_4$, $AgNO_3$, and C. Platycladi solutions were perfused separately at the same flow rate into the microfluidic reactor and heated in a glycerin bath at 90ºC. The reaction product was promptly collected and placed in an ice

bath on completion of the reaction. The size, morphology, and structure of the nanoparticles were characterized by TEM, UV-vis spectroscopy, and XRD. The TEM images of the nanoparticles show high monodispersity of the synthesized nanoparticles [Figure 8(C)].

Periyasamy et al. used a polytetrafluoroethylene (PTFE) helical tubular capillary microfluidic reactor to synthesize SnO_2 nanoparticles [122]. The setup uses a syringe pump to inject $SnCl_4.5H_2O$ and NaOH aqueous solutions into the microfluidic reactor, where they meet a T-junction. The microfluidic reactor was kept in an oil bath at 90^{o}C, and the reactions were let to happen for 5 minutes. The reaction products are quenched at the outlet using an ice bath and dried overnight in a desiccator. TEM images [Figure 8(D)] were used to determine the size, shape morphology, crystallinity, and agglomeration behavior of the resulting SnO_2 nanoparticles.

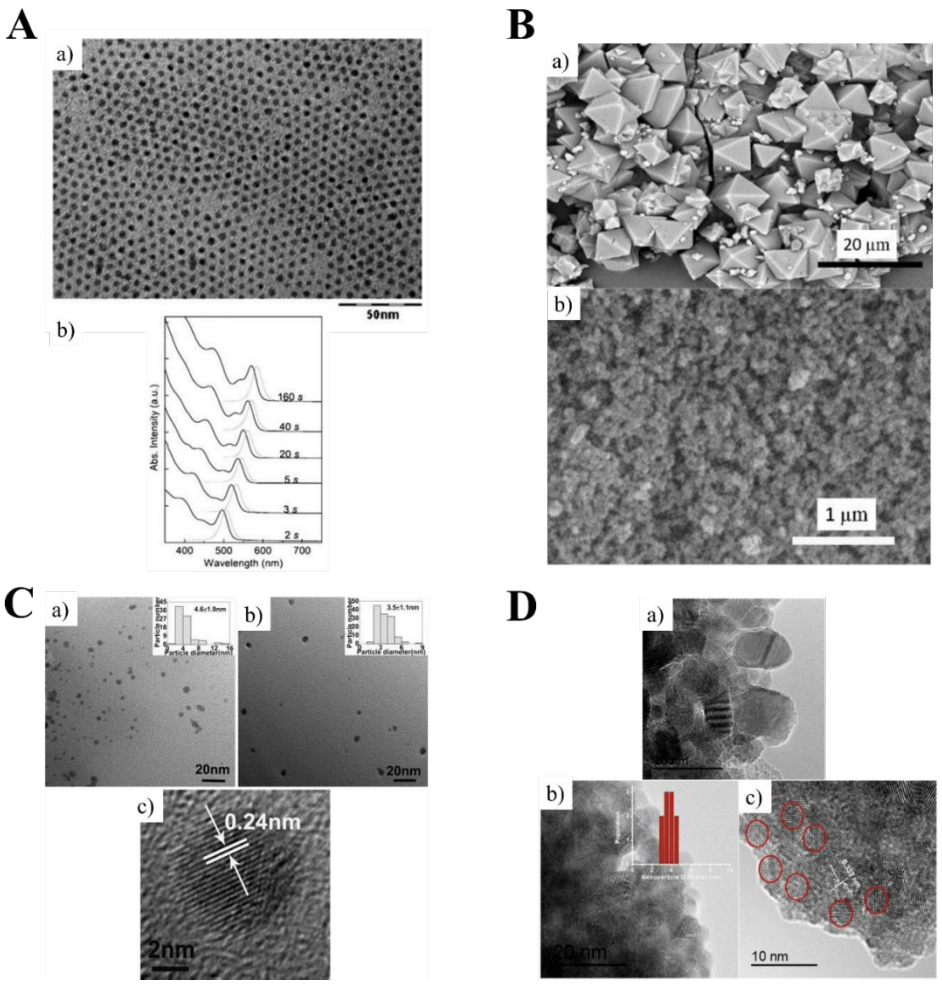

Figure 8. Characterization of nanoparticle size synthesized by utilizing temperature-assisted microfluidic reactors. (A) TEM image of quantum dot nanoparticles synthesized with a residence time of 160 sec (a), Absorption-emission spectra of the nanoparticles synthesized with different residence times in the capillary microfluidic reactor (b) [121]. (Reproduced from Ref. [121] with permission from the Royal Society of Chemistry.) (B) SEM images of the UiO-66 nanoparticles synthesized by (a) solvothermal process, (b) microfluidic reactor [117]. (Reproduced from Ref. [117] with permission from the Elsevier.) (C) TEM images of the synthesized Au-Ag bimetallic nanoparticles in the microfluidic reactor with Au/Ag molar ratios (a) 1:1, and (b) 1:2, and (c) lattice plane characterization (d-spacing) of the nanoparticle crystals using high resolution TEM (HRTEM) [118]. (Reproduced from Ref. [118] with permission from the Springer Nature.) (D) TEM image (a), size distribution (b), and lattice plane characterization (c) of the synthesized SnO_2 nanoparticles [122]. (Reproduced from Ref. [122] with permission from the Elsevier.)

4.4. Magnetic-assisted microfluidic reactor Approach to Develop Nanoparticles

This kind of micromixer utilizes an external magnetic field to mix fluids [123–127]. The external applied magnetic field can be rotational, uni, bi-directional, or simply an alternating magnetic field.

Unlike acoustic, thermal, and pressure-driven mixers, magnetically actuated mixers are better for mixing as the energy provided does not hamper the reaction process by generating heat or pressure. Hence most of the conventional reaction is carried out using a magnetically actuated stirrer and this translated at micro-scale facilitates higher mixing.

In a study by Kamat et al., chitosan nanoparticles were synthesized using a microfluidic reactor with magnetic microneedles [Figure 9 (A)] [54]. The micromagnetic needles were fabricated using PDMS and iron oxide, which actuated in an external magnetic field, causing high turbulence. The microfluidic reactor has two inlets for chitosan and tripolyphosphate (TPP), respectively, and two different mixing chambers with magnetic actuators connected in series for higher mixing efficiency. With this microfluidic reactor, nanoparticles of 130 ± 9 nm size could be synthesized, whereas under the same conditions, the conventional batch production produced large nanoparticles (250 ± 27 nm). The size of the nanoparticles was measured using a nanoparticle tracking analyzer. Also, the zeta potential results indicated that the nanoparticles synthesized by this microfluidic reactor showed higher stability than the nanoparticles synthesized using batch production. TEM was utilized to characterize the morphology of the nanoparticles [Figure 10(A)]. This microfluidic reactor was also utilized to synthesize drug (amphotericin B) entrapped chitosan nanoparticles. Two different methods were used for entrapping the drugs. In the first method, the drug was mixed with TPP and allowed to be perfused through one inlet, and in the other inlet, chitosan solution was perfused. The nanoparticles with drugs were synthesized in the first chamber, and in the second chamber, they were more mixed. In the second approach, the drug was induced to already formed chitosan nanoparticles in another chamber through another inlet. The drug entrapment increased by almost 40% compared to the first approach. The nanoparticle showed nearly 52% release of drugs within 120 h, which became approximately 80% within 336 h.

Same research group utilized a micro-magnetic stir bar for mixing was carried out to synthesize chitosan nanoparticles [128]. Size measurement based on DLS method and SEM images analysis show that highly monodisperse chitosan nanoparticles were synthesized using microfluidic reactor [Figure 10(B)]. In situ antifungal drug amphotericin was also loaded on these nanoparticles. The micromixer was fabricated using PDMS with circular channels (inlets and outlets) and the cylindric chamber where the reaction takes place. A micromagnetic needle was manufactured using PDMS and Iron oxide, which actuated in the presence of an external rotating magnetic field, causing high turbulence. The well-controlled microfluidic reactor-based mixing generated highly monodisperse particles with higher drug entrapment of around 80% than conventionally achieved 65%.

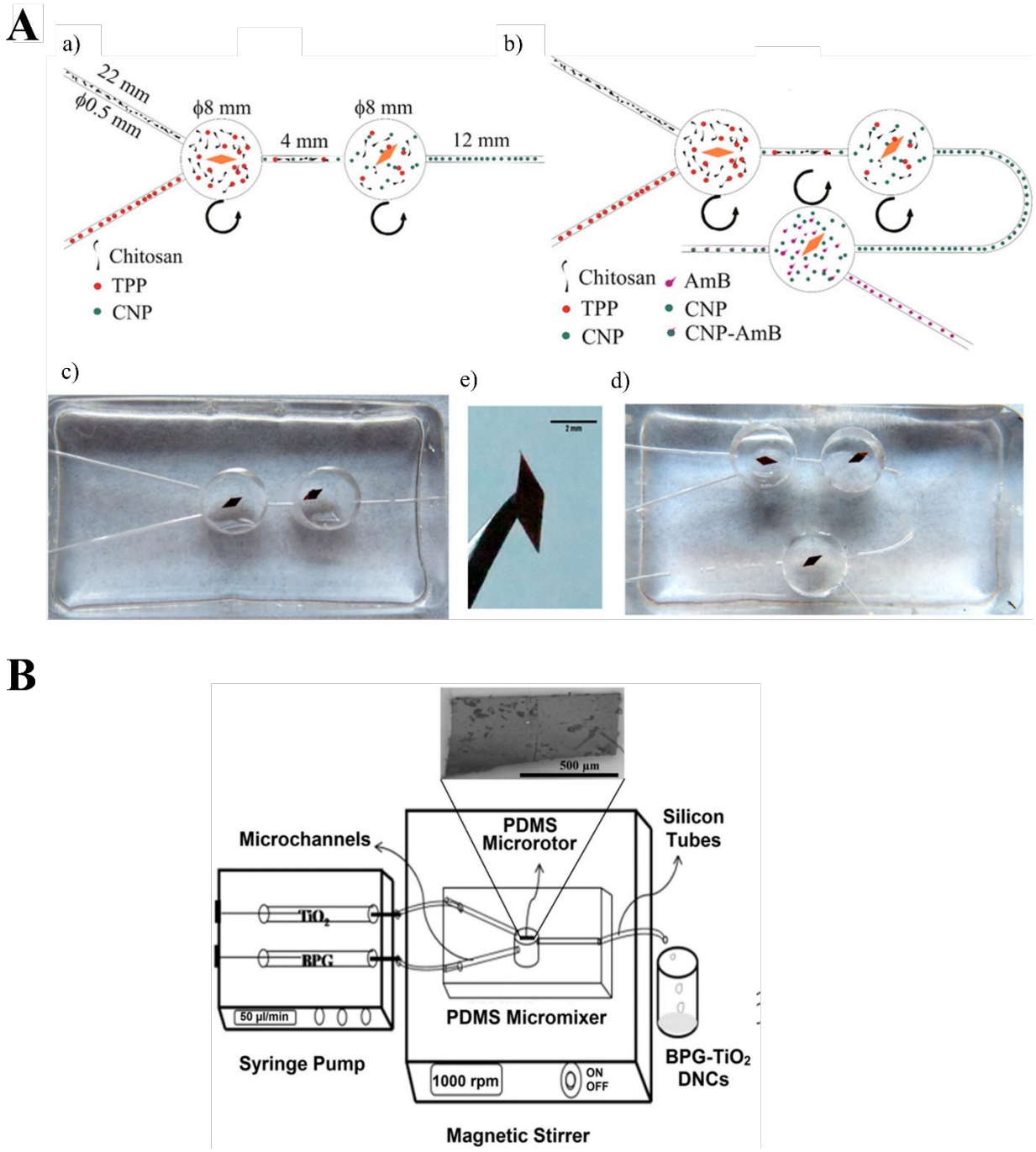

Figure 9. Magnetic field-assisted microfluidic reactor for nanoparticle synthesis. (A) Schematic representation and optical image of fabricated microfluidic reactor chip for (a, c) chitosan nanoparticles synthesis by the 2-chamber method, (b, d) drug loading by 3-chamber method; (e) Rhombic magnetic needle [54]. (Reproduced from Ref. [54] with permission from the American Chemical Society.) (B) Schematic of the synthesis of BPG-TiO_2 nanoparticles using magnetic field-assisted micromixer [129]. (Reproduced from Ref. [129] with permission from the Elsevier.)

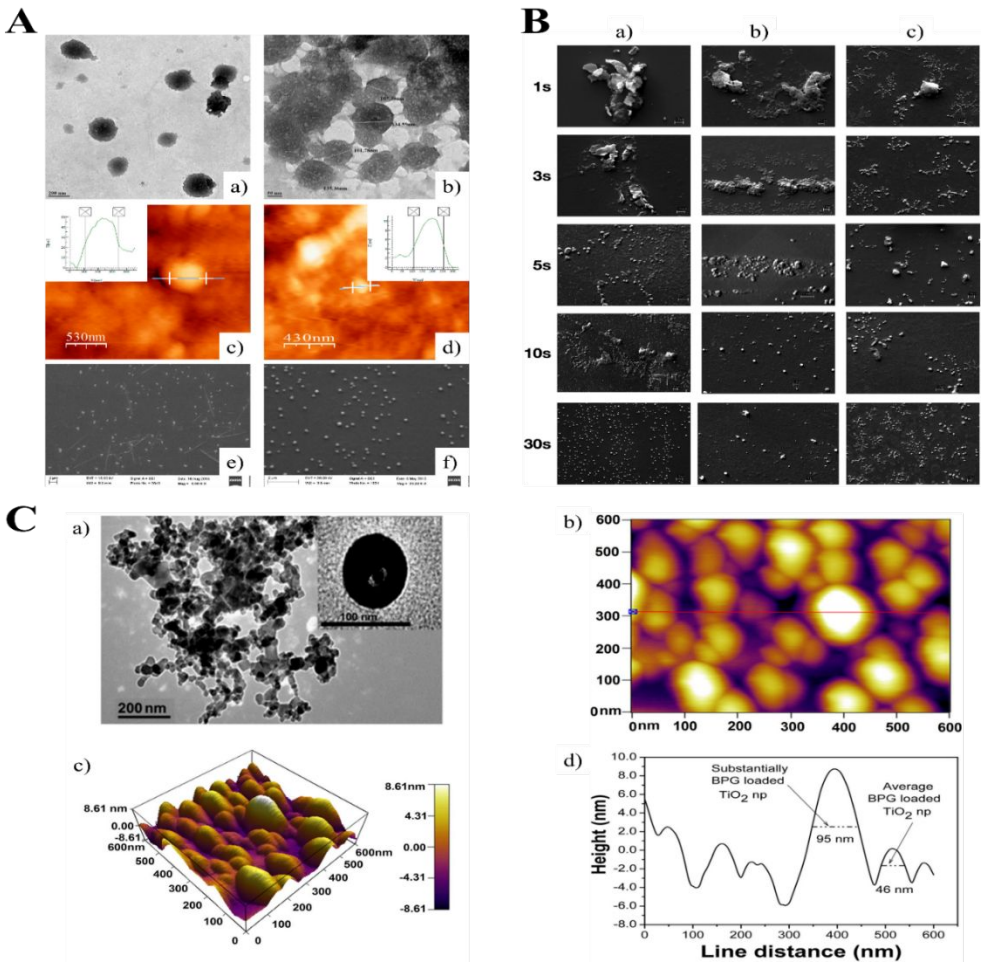

Figure 10. Characterization of nanoparticle synthesized by utilizing magnetic field-assisted microfluidic reactor. (A) TEM images (a, b), AFM images, and size distribution from AFM of chitosan nanoparticles synthesized by using microfluidic reactor (c,d), and SEM images of nanoparticles synthesized by using magnetic field-assisted microfluidic reactor (e), conventional batch production (f) [54]. (Reproduced from Ref. [54] with permission from the American Chemical Society.) (B) SEM images of the chitosan nanoparticles formed at different reaction times and at different temperatures: (a) 4 ºC, (b) 27 ºC, and (c) 35 ºC [128]. (Reproduced from Ref. [128] with permission from the Springer Nature.) (C) TEM image of BPG loaded TiO_2 nanoparticles (a), AFM image of the nanoparticles with a horizontal line showing the amount of BPG loading on TiO_2 nanoparticles in figure d (b), The 3D surface topography of the BPG-TiO_2 nanoparticles, and AFM results showing the amount of BPG loading on the TiO_2 nanoparticles (d) [129]. (Reproduced from Ref. [129] with permission from the Elsevier.)

TiO_2 nanoparticles were complexed with one of the forms of penicillin [Benzathine Penicillin G tetrahydrate (BPG)] was carried out using a similar micromixer in the study by Veldurthi et al

[Figure 9(B)] [129]. The interaction between nanoparticles and BPG was purely based on electrostatic, leading to the formation of the drug-nanoparticle complex. The amount of BPG in the TiO_2 nanoparticles was measured from thermogravimetric analysis (TGA). TEM was used to find the distribution of BPG on the TiO_2 nanoparticles [Figure 10(C)]. And atomic force microscopy (AFM) was utilized to characterize the surface topography of the BPG-loaded TiO_2 nanoparticles [Figure 10(C)].

5. Challenges, and future perspectives

Although microfluidic reactors are a promising tool, yet several key aspects are yet to be fully explored. The goal of any chemical reaction is to maximize the product yield/activity/reaction by tailoring reaction parameters in the most optimum configuration. Microfluidic reactions are dominated by laminar flow which is advantageous for certain applications such as separation technologies but not for chemical reactions and therefore homogenous mixing in microfluidic devices remains a major challenge. This majorly affect synthesis of nanoparticles. In a non-homogeneous mixing multiple random nuclei sites are generated which eventually grow at different rates leading to polydisperse preparation. In an ideal scenario precursor and linker/catalyst molecule should react in controlled fix stoichiometry for a definite time to yield monodispersed nanoparticles. This can only happen when nucleation and growth are separated (non-gradient environment) by exerting high control on reaction time or residence time which is far better achieved using active microfluidic reactors. With respect to, passive microfluidic reactors which require complex geometry to induce disturbance within the fluids for mixing can lead to gradients and multiple nucleation sites leading to polydispersity. This also leads to incomplete reactions, generation of byproducts and intermediary precursors compounds decreasing efficiency of reaction. However, using microfluidic active reactors several of these challenges can be answered

yet due to their complicated integration, active microfluidic reactors have not been utilized extensively to synthesize nanoparticles and even less for biomedical applications. The current reactors largely depend on flow rate control using peristaltic or syringe pumps limiting their portability and operation. Another key challenge in commercialization of this technology is the limited current understanding for scaling up the process.

In light of the current challenges, If the fabrication process can be streamlined, microfluidic reactors can be automated and have the potential to mass-produce monodispersed nanoparticles suitable for biomedical applications. Microfluidic technologies have provided the ability to handle and manipulate liquids to exert control on reactants, mixing efficiency and reaction time for optimizing chemical reactions. In writing this review, it is our intention to motivate further research in the area of active microfluidic reactors.

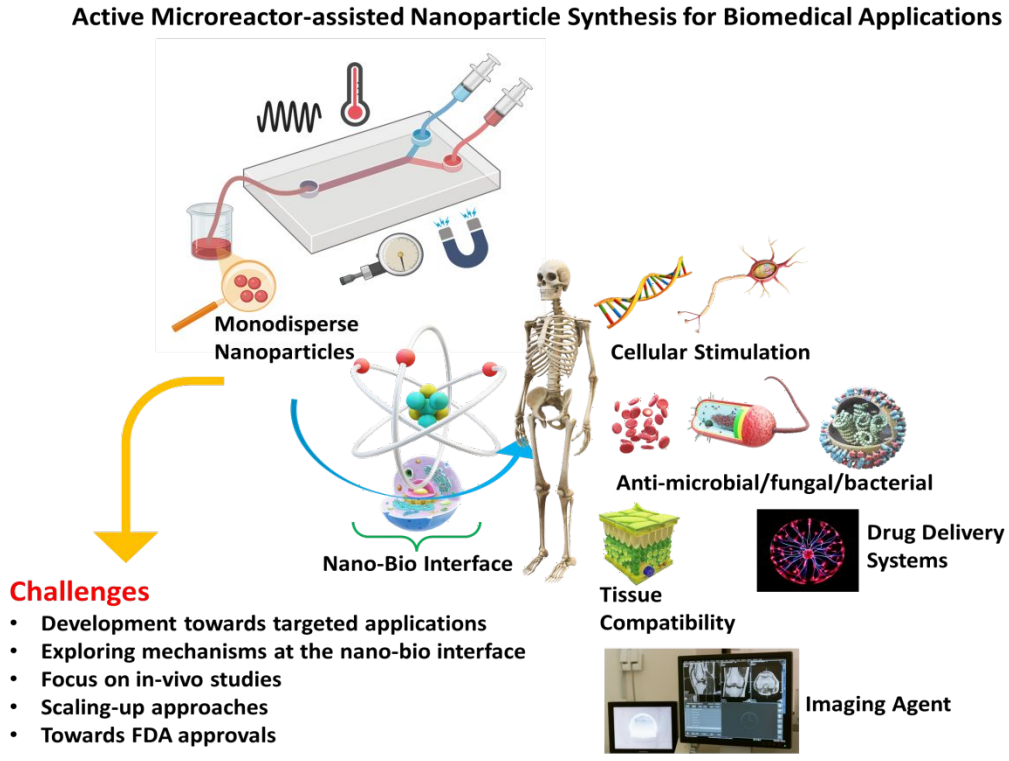

Figure 11. Synthesis of nanoparticles with the active microfluidic reactor route, their applications in biomedicine, and the potential challenges

5. Conclusion

In conclusion, the technique for synthesizing nanoparticles using microfluidic reactors has transformed the chemistry of nanoparticle synthesis. Employing active microfluidic reactors to manipulate and control the nucleation and growth of nanoparticles, it is now possible to generate highly monodisperse nanoparticles used as efficient drug delivery vehicles. Active micromixers using external energy sources can be controlled far better, allowing nanoparticle size to be precisely adjusted. In addition, this kind of microfluidic reactor is able to create a comparatively higher Reynolds number which in certain geometries can increase mixing in a small volume by reducing the symmetry of Dean vortices. In addition, as a result of the use of an external energy source, these microfluidic reactors need fewer solutions and enable quicker mixing, hence reducing the volume of expensive precursors and the time necessary for nanoparticle manufacturing.

This review, to the best of our knowledge, is the first of its kind to describe in detail the different kinds of active microfluidic reactors used to synthesize nanoparticles for biomedical applications. With the potential to produce extremely monodisperse particles, active microfluidic reactors can be used as a bedside technology for the synthesis and delivery of nano-drug formulations on demand. This approach can also be used to manufacture nanoparticles containing personalized and multifunctional medications. For example, vaccines are crucial for acquiring protection against a variety of diseases. With monodisperse nanoparticles generated by active microfluidic reactors, nano vaccines can be administered with increased efficacy. These technologies can also be effectively applied to the continuous administration of anti-cancer drugs, such as insulin injections. Using such a platform combined with a wearable smart device, more personalized drugs, and nanomedicine can be dispensed. Nanoparticles have tremendous potential in biomedicine, but there are still obstacles to overcome, such as evaluating performance in-vivo settings, obtaining US Food and Drug Administration (FDA) clearance, scaling up for developing more economic drugs, and

developing drugs for more specialized applications, etc. (Figure 11). This review's long-term objective is to encourage the use of active microfluidic reactors for a variety of biomedical applications and to overcome new obstacles in drug delivery, nanomedicine, bioimaging, biosensors, and diagnostics.

Acknowledgments

V.K. and P.D. made equal contributions to this work. V.K and P.D planned the conception and design of the review and co-wrote along with preparing the original draft. D.B and A.B performed critical revision, writing review, and editing. A.K, S.B provided the visualization, supervision, writing review, and editing. All authors offered intellectual inputs, read, and approved the manuscript.

Conflict of Interest: Authors declare no conflict of interest

References

1 Y. Badr and M. A. Mahmoud, *Crystal Research and Technology: Journal of Experimental and Industrial Crystallography*, 2006, **41**, 658–663.
2 E. P. Sajitha, V. Prasad, S. V. Subramanyam, A. K. Mishra, S. Sarkar and C. Bansal, *Journal of Physics: Condensed Matter*, 2007, **19**, 046214–046214.
3 Q. Yu, L. Qi, R. K. Mishra, X. Zeng and A. M. Minor, *Applied Physics Letters*, 2015, **106**, 261903–261903.
4 P. Warrier and A. Teja, *Nanoscale research letters*, 2011, **6**, 1–6.
5 P. M. Tiwari, K. Vig, V. A. Dennis and S. R. Singh, *Nanomaterials*, 2011, **1**, 31–63.
6 M. Segev-Bar and H. Haick, *ACS nano*, 2013, **7**, 8366–8378.
7 D. J. de Aberasturi, A. B. Serrano-Montes and L. M. Liz-Marzán, *Advanced Optical Materials*, 2015, **3**, 602–617.
8 D. Yohan and B. D. Chithrani, *Journal of Biomedical Nanotechnology*, 2014, **10**, 2371–2392.
9 X. Chen and P. J. Dobson, in *Nanoparticles in Biology and Medicine*, Springer, 2012, pp. 103–123.
10 A. M. Skelley, O. Kirak, H. Suh, R. Jaenisch and J. Voldman, *Nature methods*, 2009, **6**, 147–152.
11 G. Linshiz, E. Jensen, N. Stawski, C. Bi, N. Elsbree, H. Jiao, J. Kim, R. Mathies, J. D. Keasling and N. J. Hillson, *Journal of biological engineering*, 2016, **10**, 1–15.

12 A. J. Demello, *Nature*, 2006, **442**, 394–402.
13 Z. Li, P. Dey and S.-J. Kim, *Sensors and Actuators B: Chemical*, 2019, **296**, 126692.
14 P. Dey, Z. Li and S.-J. Kim, 대한기계학회 춘추학술대회, 2019, 1458–1460.
15 P. Dey, T. M. Bradley and A. Boymelgreen, *bioRxiv*, 2023, 2023.01.20.524934.
16 R. W. Epps, K. C. Felton, C. W. Coley and M. Abolhasani, *Lab on a Chip*, 2017, **17**, 4040–4047.
17 N. Bourguignon, V. Kamat, M. Perez, K. Mathee, B. Lerner and S. Bhansali, *Applied Microbiology and Biotechnology*, 2022, **106**, 2729–2738.
18 N. Bourguignon, V. A. Kamat, B. Lerner, M. Perez and S. Bhansali, IOP Publishing, 2019, pp. 2103–2103.
19 V. A. Kamat, T. Zhukov and S. Bhansali, IOP Publishing, 2019, pp. 2102–2102.
20 V. Kamat, S. Pandey, K. Paknikar and D. Bodas, *Biosensors and Bioelectronics*, 2018, **99**, 62–69.
21 J. R. Burns and C. Ramshaw, *Chemical Engineering Research and Design*, 1999, **77**, 206–211.
22 B. P. Mason, K. E. Price, J. L. Steinbacher, A. R. Bogdan and D. T. McQuade, *Chemical reviews*, 2007, **107**, 2300–2318.
23 X. Zhang, S. Stefanick and F. J. Villani, *Organic process research & development*, 2004, **8**, 455–460.
24 C. G. Frost and L. Mutton, *Green Chemistry*, 2010, **12**, 1687–1703.
25 J. Wagner and J. M. Köhler, *Nano letters*, 2005, **5**, 685–691.
26 B. Ahmed-Omer, J. C. Brandt and T. Wirth, *Organic & biomolecular chemistry*, 2007, **5**, 733–740.
27 T. Frommelt, M. Kostur, M. Wenzel-Schäfer, P. Talkner, P. Hänggi and A. Wixforth, *Physical review letters*, 2008, **100**, 034502–034502.
28 E. Tripathi, P. K. Patowari and S. Pati, *Chemical Engineering and Processing-Process Intensification*, 2021, **162**, 108335.
29 T. J. Johnson, D. Ross and L. E. Locascio, *Analytical chemistry*, 2002, **74**, 45–51.
30 V. Mengeaud, J. Josserand and H. H. Girault, *Analytical chemistry*, 2002, **74**, 4279–4286.
31 G. Cai, L. Xue, H. Zhang and J. Lin, *Micromachines*, 2017, **8**, 274.
32 M. Bayareh, M. N. Ashani and A. Usefian, *Chemical Engineering and Processing-Process Intensification*, 2020, **147**, 107771–107771.
33 K. Ward and Z. H. Fan, *Journal of Micromechanics and Microengineering*, 2015, **25**, 094001.
34 L. Capretto, W. Cheng, M. Hill and X. Zhang, *Microfluidics: technologies and applications*, 2011, 27–68.
35 N.-T. Nguyen and Z. Wu, *Journal of micromechanics and microengineering*, 2004, **15**, R1.
36 A. V. Minakov, V. Y. Rudyak, A. A. Gavrilov and A. A. Dekterev, *Thermophysics and Aeromechanics*, 2012, **19**, 385–395.
37 G. Kunti, A. Bhattacharya and S. Chakraborty, *Electrophoresis*, 2017, **38**, 1310–1317.
38 C.-Y. Chen, C.-Y. Chen, C.-Y. Lin and Y.-T. Hu, *Lab on a Chip*, 2013, **13**, 2834–2839.
39 K. Boonyaphon, Z. Li, G. Kim, C. S. Lim and S.-J. Kim, *Sensors and Actuators B: Chemical*, 2018, **277**, 431–436.
40 Y.-H. Lin, C.-C. Wang and K. F. Lei, *Biomedical microdevices*, 2014, **16**, 199–207.
41 W.-B. Lee, Y.-H. Chen, H.-I. Lin, S.-C. Shiesh and G.-B. Lee, *Sensors and Actuators B: Chemical*, 2011, **157**, 710–721.
42 J. Kim, D. Taylor, N. Agrawal, H. Wang, H. Kim, A. Han, K. Rege and A. Jayaraman, *Lab on a Chip*, 2012, **12**, 1813–1822.

43 K. Petkovic, G. Metcalfe, H. Chen, Y. Gao, M. Best, D. Lester and Y. Zhu, *Lab on a Chip*, 2017, **17**, 169–177.
44 V. K. LaMer and R. H. Dinegar, *Journal of the american chemical society*, 1950, **72**, 4847–4854.
45 T. Sugimoto, *Monodispersed particles*, Elsevier, 2019.
46 S. Navaladian, B. Viswanathan, R. Viswanath and T. Varadarajan, *Nanoscale research letters*, 2007, **2**, 44–48.
47 X. Ji, X. Song, J. Li, Y. Bai, W. Yang and X. Peng, *Journal of the American Chemical Society*, 2007, **129**, 13939–13948.
48 S. Watanabe, S. Ohsaki, A. Fukuta, T. Hanafusa, K. Takada, H. Tanaka, T. Maki, K. Mae and M. T. Miyahara, *Advanced Powder Technology*, 2017, **28**, 3104–3110.
49 J. M. Köhler, L. Abahmane, J. Wagner, J. Albert and G. Mayer, *Chemical Engineering Science*, 2008, **63**, 5048–5055.
50 M. E. Potter, D. J. Stewart, A. E. Oakley, R. P. Boardman, T. Bradley, P. J. A. Sazio and R. Raja, *ACS Photonics*, 2020, **7**, 714–722.
51 S. Tao, M. Yang, H. Chen and G. Chen, *ACS Sustainable Chemistry & Engineering*, 2018, **6**, 8719–8726.
52 E. Lobry, F. Jasinski, M. Penconi, A. Chemtob, C. Croutxé-Barghorn, E. Oliveros, A. M. Braun and A. Criqui, *RSC Advances*, 2014, **4**, 43756–43759.
53 A. K. Yadav, M. J. Barandiaran and J. C. de la Cal, *Chemical engineering journal*, 2012, **198**, 191–200.
54 V. Kamat, I. Marathe, V. Ghormade, D. Bodas and K. Paknikar, *ACS applied materials & interfaces*, 2015, **7**, 22839–22847.
55 K.-I. Min, H.-J. Lee and D.-P. Kim, *Lab on a Chip*, 2014, **14**, 3987–3992.
56 A. Dobhal, A. Kulkarni, P. Dandekar and R. Jain, *Journal of Materials Chemistry B*, 2017, **5**, 3404–3417.
57 J. D. Winterton, D. R. Myers, J. M. Lippmann, A. P. Pisano and F. M. Doyle, *Journal of Nanoparticle Research*, 2008, **10**, 893–905.
58 A. Abou-Hassan, O. Sandre and V. Cabuil, *Angewandte Chemie International Edition*, 2010, **49**, 6268–6286.
59 B. J. Kirby, *Micro-and nanoscale fluid mechanics: transport in microfluidic devices*, Cambridge university press, 2010.
60 C. C. Miller, *Proceedings of the Royal Society of London. Series A, Containing Papers of a Mathematical and Physical Character*, 1924, **106**, 724–749.
61 S. T. Selvan, T. T. Y. Tan, D. K. Yi and N. R. Jana, *Langmuir*, 2010, **26**, 11631–11641.
62 N. H. A. Le, H. Deng, C. Devendran, N. Akhtar, X. Ma, C. Pouton, H.-K. Chan, A. Neild and T. Alan, *Lab on a Chip*, 2020, **20**, 582–591.
63 S. Adepu and S. Ramakrishna, *Molecules*, 2021, **26**, 5905–5905.
64 K. Cho, X. U. Wang, S. Nie and D. M. Shin, *Clinical cancer research*, 2008, **14**, 1310–1316.
65 S. Gelperina, K. Kisich, M. D. Iseman and L. Heifets, *American journal of respiratory and critical care medicine*, 2005, **172**, 1487–1490.
66 R. Singh and J. W. Lillard Jr, *Experimental and molecular pathology*, 2009, **86**, 215–223.
67 M. Bañobre-López, A. Teijeiro and J. Rivas, *Reports of Practical Oncology & Radiotherapy*, 2013, **18**, 397–400.
68 A. B. Salunkhe, V. M. Khot and S. Pawar, *Current topics in medicinal chemistry*, 2014, **14**, 572–594.
69 G. Chen, I. Roy, C. Yang and P. N. Prasad, *Chemical reviews*, 2016, **116**, 2826–2885.

70 S. K. Nune, P. Gunda, P. K. Thallapally, Y.-Y. Lin, M. Laird Forrest and C. J. Berkland, *Expert opinion on drug delivery*, 2009, **6**, 1175–1194.
71 S. J. Douglas, S. S. Davis and L. Illum, *Critical reviews in therapeutic drug carrier systems*, 1987, **3**, 233–261.
72 P. Couvreur, *Advanced drug delivery reviews*, 2013, **65**, 21–23.
73 G. Ajnai, A. Chiu, T. Kan, C.-C. Cheng, T.-H. Tsai and J. Chang, *Journal of Experimental & Clinical Medicine*, 2014, **6**, 172–178.
74 S. R. Dave and X. Gao, *Wiley Interdisciplinary Reviews: Nanomedicine and Nanobiotechnology*, 2009, **1**, 583–609.
75 L. Kafrouni and O. Savadogo, *Progress in Biomaterials*, 2016, **5**, 147–160.
76 E. Kita, T. Oda, T. Kayano, S. Sato, M. Minagawa, H. Yanagihara, M. Kishimoto, C. Mitsumata, S. Hashimoto and K. Yamada, *Journal of Physics D: Applied Physics*, 2010, **43**, 474011–474011.
77 N. Erathodiyil and J. Y. Ying, *Accounts of chemical research*, 2011, **44**, 925–935.
78 X. Luo, A. Morrin, A. J. Killard and M. R. Smyth, *Electroanalysis: An International Journal Devoted to Fundamental and Practical Aspects of Electroanalysis*, 2006, **18**, 319–326.
79 H. Malekzad, P. S. Zangabad, H. Mirshekari, M. Karimi and M. R. Hamblin, *Nanotechnology reviews*, 2017, **6**, 301–329.
80 G. Doria, J. Conde, B. Veigas, L. Giestas, C. Almeida, M. Assunção, J. Rosa and P. V. Baptista, *Sensors*, 2012, **12**, 1657–1687.
81 L. M. Rossi, A. D. Quach and Z. Rosenzweig, *Analytical and Bioanalytical Chemistry*, 2004, **380**, 606–613.
82 K. Chatterjee, S. Sarkar, K. J. Rao and S. Paria, *Advances in colloid and interface science*, 2014, **209**, 8–39.
83 M. R. Ghazanfari, M. Kashefi, S. F. Shams and M. R. Jaafari, *Biochemistry research international*.
84 L. S. Ganapathe, M. A. Mohamed, R. Mohamad Yunus and D. D. Berhanuddin, *Magnetochemistry*, 2020, **6**, 68–68.
85 J. Liu and Q. Peng, *Acta biomaterialia*, 2017, **55**, 13–27.
86 K. McNamara and S. A. Tofail, *Advances in Physics: X*, 2017, **2**, 54–88.
87 E. H. Jeong, G. Jung, C. A. Hong and H. Lee, *Archives of pharmacal research*, 2014, **37**, 53–59.
88 L. Dykman and N. Khlebtsov, *Chemical Society Reviews*, 2012, **41**, 2256–2282.
89 A.-C. Burduşel, O. Gherasim, A. M. Grumezescu, L. Mogoantă, A. Ficai and E. Andronescu, *Nanomaterials*, 2018, **8**, 681–681.
90 R. Shanmuganathan, I. Karuppusamy, M. Saravanan, H. Muthukumar, K. Ponnuchamy, V. S. Ramkumar and A. Pugazhendhi, *Current pharmaceutical design*, 2019, **25**, 2650–2660.
91 A. Haider and I.-K. Kang, *Advances in materials science and engineering*.
92 S. Y. Srinivasan, K. M. Paknikar, D. Bodas and V. Gajbhiye, *Nanomedicine*, 2018, **13**, 1221–1238.
93 Q. Y. Tamboli, S. M. Patange, Y. K. Mohanta, R. Sharma and K. R. Zakde, *Journal of Nanomaterials*.
94 M. S. Shakil, M. S. Bhuiya, M. R. Morshed, G. Babu, M. S. Niloy, M. S. Hossen and M. A. Islam, *Current medicinal chemistry*, 2023, **30**, 1756–1775.
95 J. Mou, Y. Ren, J. Wang, C. Wang, Y. Zou, K. Lou, Z. Zheng and D. Zhang, *Microfluidics and Nanofluidics*, 2022, **26**, 25.
96 V. Sebastian, *Nanoscale*, 2022, **14**, 4411–4447.

97 Z. Chen, Z. Pei, X. Zhao, J. Zhang, J. Wei and N. Hao, *Chemical Engineering Journal*, 2022, **433**, 133258.
98 X. Zhao, Z. Chen, Y. Qiu and N. Hao, *Materials Advances*, 2023, **4**, 988–994.
99 A. Bendre, M. P. Bhat, K.-H. Lee, T. Altalhi, M. A. Alruqi and M. Kurkuri, *Materials Today Advances*, 2022, **13**, 100205.
100 W. Lin, S. Lai, D. Lu, Q. Zhang, X. Lin, J. Lin, J. Wang and Z. Huang, *Sensors and Actuators B: Chemical*, 2022, **356**, 131361.
101 P. Huang, S. Zhao, H. Bachman, N. Nama, Z. Li, C. Chen, S. Yang, M. Wu, S. P. Zhang and T. J. Huang, *Advanced Science*, 2019, **6**, 1900913–1900913.
102 A. Pourabed, T. Younas, C. Liu, B. K. Shanbhag, L. He and T. Alan, *Journal of Colloid and Interface Science*, 2021, **585**, 229–236.
103 N. Hao, P. Liu, H. Bachman, Z. Pei, P. Zhang, J. Rufo, Z. Wang, S. Zhao and T. J. Huang, *ACS nano*, 2020, **14**, 6150–6163.
104 M. R. Rasouli and M. Tabrizian, *Lab on a Chip*, 2019, **19**, 3316–3325.
105 H. M. Xia, Y. P. Seah, Y. C. Liu, W. Wang, A. G. G. Toh and Z. P. Wang, *Microfluidics and Nanofluidics*, 2015, **19**, 283–290.
106 A. Pourabed, J. Brenker, T. Younas, L. He and T. Alan, *Ultrasonics Sonochemistry*, 2022, **83**, 105936–105936.
107 Y. Abbas, J. Miwa, R. Zengerle and F. Von Stetten, *Micromachines*, 2013, **4**, 80–89.
108 G. Liu, X. Yang, Y. Li, Z. Yang, W. Hong and J. Liu, *Advances in Materials Science and Engineering*.
109 O. Français, M.-C. Jullien, L. Rousseau, P. Poulichet, S. Desportes, A. Chouai, J.-P. Lefevre and J. Delaire, *arXiv preprint arXiv:0711.3290*.
110 C. Huang and C. Tsou, *Sensors and actuators A: Physical*, 2014, **210**, 147–156.
111 H. Yang, W. Luan, R. Cheng, H. Chu and S. Tu, *Journal of Nanoparticle Research*, 2011, **13**, 3335–3344.
112 X. Wang, X. Ma, L. An, X. Kong, Z. Xu and J. Wang, *Science China Chemistry*, 2013, **56**, 799–805.
113 W.-B. Lee, C.-H. Weng, F.-Y. Cheng, C.-S. Yeh, H.-Y. Lei and G.-B. Lee, *Biomedical microdevices*, 2009, **11**, 161–171.
114 F. Zhang, H. Chen, B. Chen and J. Wu, *Advances in Mechanical Engineering*, 2016, **8**, 1687814016646264–1687814016646264.
115 K.-R. Huang, J.-S. Chang, S. D. Chao, T.-S. Wung and K.-C. Wu, *Japanese Journal of Applied Physics*, 2012, **51**, 047002–047002.
116 S.-J. Kim, F. Wang, M. A. Burns and K. Kurabayashi, *Analytical chemistry*, 2009, **81**, 4510–4516.
117 S. Tai, W. Zhang, J. Zhang, G. Luo, Y. Jia, M. Deng and Y. Ling, *Microporous and Mesoporous Materials*, 2016, **220**, 148–154.
118 H. Liu, J. Huang, D. Sun, T. Odoom-Wubah, J. Li and Q. Li, *Journal of nanoparticle research*, 2014, **16**, 1–9.
119 K. Sue, T. Sato, S. Kawasaki, Y. Takebayashi, S. Yoda, T. Furuya and T. Hiaki, *Industrial & Engineering Chemistry Research*, 2010, **49**, 8841–8846.
120 K. Y. Park, M. Ullmann, Y. J. Suh and S. K. Friedlander, *Journal of Nanoparticle Research*, 2001, **3**, 309–319.
121 A. M. Nightingale and J. C. de Mello, *Journal of Materials Chemistry*, 2010, **20**, 8454–8463.

122 M. Periyasamy, A. Saha, S. Sain, M. Mandal, U. Sengupta and A. Kar, *Journal of Environmental Chemical Engineering*, 2020, **8**, 104604–104604.
123 L.-H. Lu, K. S. Ryu and C. Liu, *Journal of microelectromechanical systems*, 2002, **11**, 462–469.
124 L. M. Fu, C. H. Tsai, K. P. Leong and C. Y. Wen, *Physics Procedia*, 2010, **9**, 270–273.
125 C. Wen, C. Yeh, C. Tsai and L. Fu, *Electrophoresis*, 2009, **30**, 4179–4186.
126 H.-X. Zhang, J.-X. Wang, L. Shao and J.-F. Chen, *Industrial & engineering chemistry research*, 2010, **49**, 4156–4161.
127 K. S. Ryu, K. Shaikh, E. Goluch, Z. Fan and C. Liu, *Lab on a Chip*, 2004, **4**, 608–613.
128 V. Kamat, D. Bodas and K. Paknikar, *Scientific reports*, 2016, **6**, 1–4.
129 N. Veldurthi, P. Ghoderao, S. Sahare, V. Kumar, D. Bodas, A. Kulkarni and T. Bhave, *Materials Science and Engineering: C*, 2016, **68**, 455–464.
130 M. J. Lim, N. N. M. Shahri, H. Taha, A. H. Mahadi, E. Kusrini, J. W. Lim and A. Usman, *Carbohydrate polymers*, 2021, **260**, 117806.
131 M. Pourmadadi, E. Rahmani, A. Shamsabadipour, S. Mahtabian, M. Ahmadi, A. Rahdar and A. M. Díez-Pascual, *Nanomaterials*, 2022, **12**, 3873.
132 S. Jafari, B. Mahyad, H. Hashemzadeh, S. Janfaza, T. Gholikhani and L. Tayebi, *International journal of nanomedicine*, 2020, 3447–3470.
133 M. M. Kumari, J. Jacob and D. Philip, *Spectrochimica Acta Part A: Molecular and Biomolecular Spectroscopy*, 2015, **137**, 185–192.
134 S. Singkammo, A. Wisitsoraat, A. Tuantranont, S. Phanichphant and C. Liewhiran, *Applied Surface Science*, 2018, **458**, 281–292.